SUPPLEMENTARY INFORMATION

Parallel processing of visual space by neighboring neurons in mouse visual cortex

Spencer L. Smith and Michael Häusser
Wolfson Institute for Biomedical Research, University College London

Contents Page

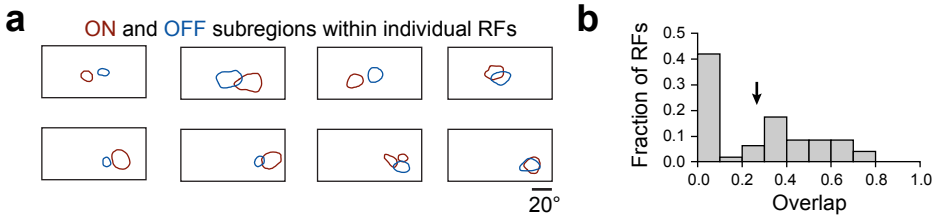

Supplementary Figure 1. Overlap of ON and OFF subregions in single receptive fields

(a) Receptive fields from eight example cells are shown, each with both the ON and OFF subregions indicated. (b) The overlap between the ON and OFF subregion in individual receptive fields was low, indicating that these neurons were mostly simple cells. The arrow indicates the mean of the distribution.

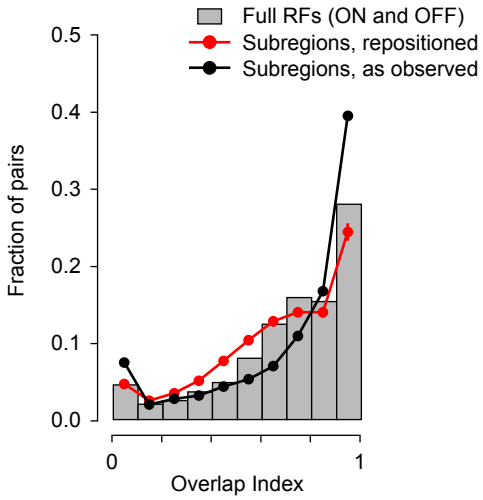

Supplementary Figure 2. Overlap of full receptive fields

The gray bars show the distribution of overlap of full receptive fields (i.e., both the ON and OFF subregion together) between pairs of cells. The distribution of overlaps more closely follows that of the RF subregions after random repositioning. By contrast, the distribution of overlaps of RF subregions as they are observed, shows a clear trend toward very high overlap.

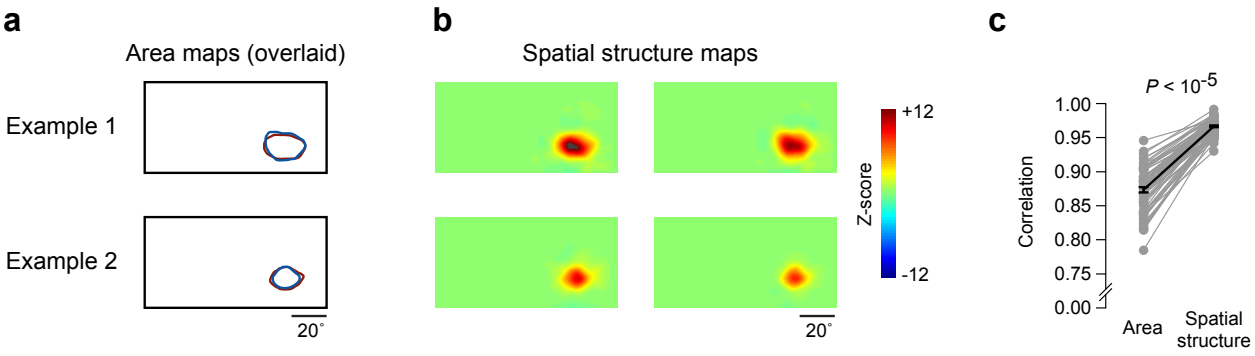

Supplementary Figure 3. RF subregions share not only an area of visual space, but spatial structure as well

In order to explore the internal structure of shared RF subregions, we computed pair-wise image correlation coefficients. (a) Two example pairs of subregions show the typical high degree of overlap in their area maps. (b) The spatial structure maps for these pairs of subregions (the filtered and z scored spike-triggered stimulus averages) appear highly similar. The maps on the left and right of panel (b) correspond to the red and blue outlines in panel (a), respectively. (c) The image correlation for the spatial structure maps was higher than the image correlation of the area maps. This shows that shared RF subregions share not only an area of visual space, but a spatial structure within that area as well.

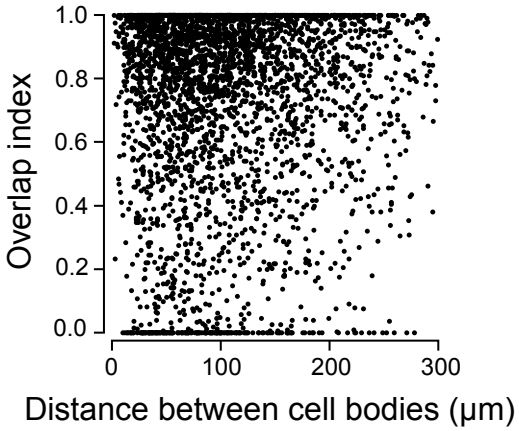

Supplementary Figure 4. Relationship between RF subunit overlap and neuron separation

Each data point represents one pair of neurons in the same population, with the distance measured between the center of their respective cell bodies plotted against the RF subregion overlap index for that pair. There was no significant correlation between the values at this scale (r = 0.036, n = 3422 pairs), despite large scale retinotopy.

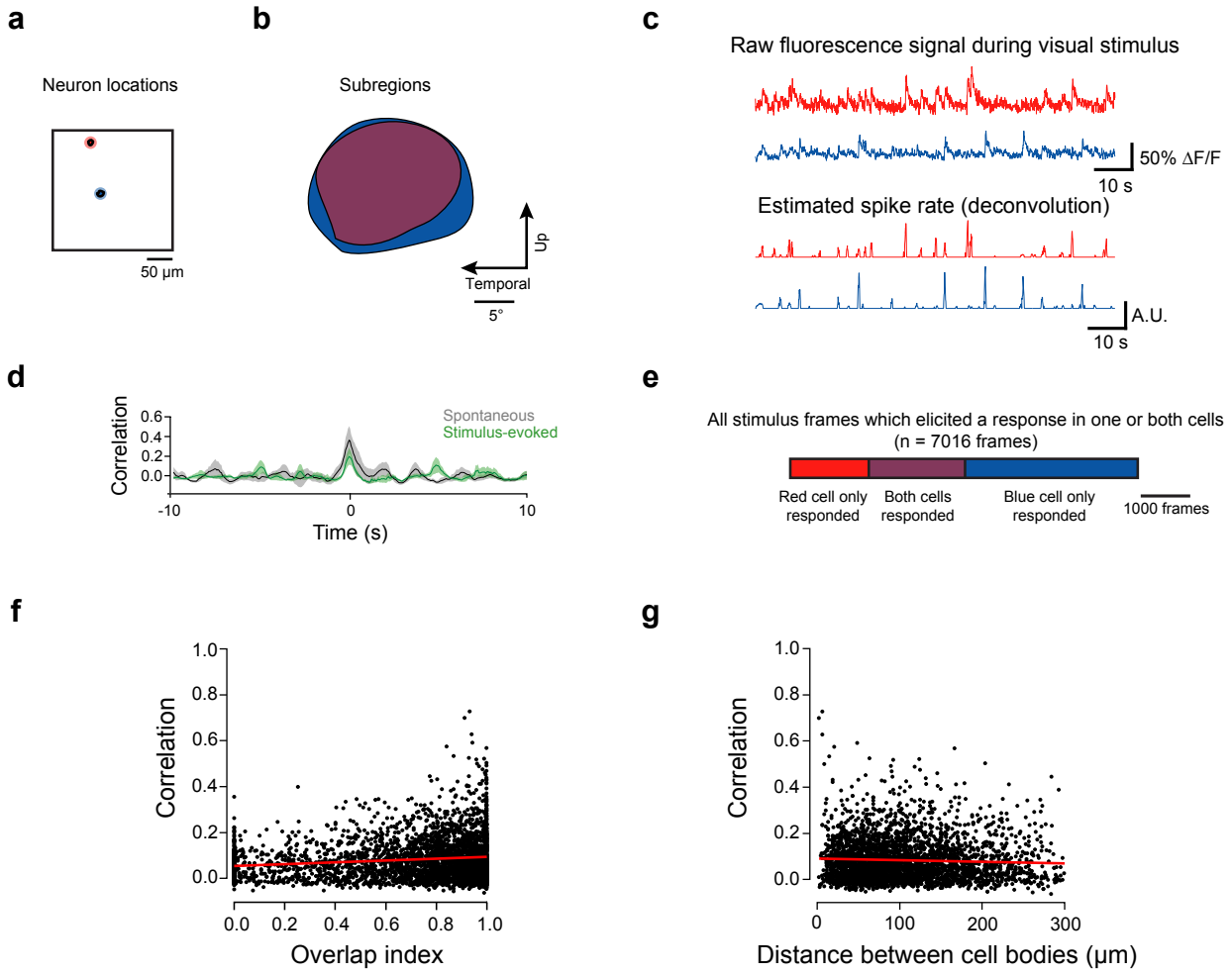

Supplementary Figure 5. Relationship between RF subunit overlap and activity correlations

(a) Two simultaneously imaged neurons (separated by over 100 µm) exhibiting shared RF subregions. (b) The subregions of the two neurons overlap completely (overlap index = 1). (c) Calcium signals and estimated spike rates from the two neurons during sparse noise visual stimulation. (d) The spike rate cross-correlation of the two neurons, while significant, was lower for stimulus-evoked than for spontaneous activity. (e) A Venn diagram shows that the neurons tended to respond to different frames of the visual stimulus. (f,g) Across the dataset, while some neurons showed substantial activity cross-correlations, there were only weak relation- ships between (f) the strength of the cross-correlation and the overlap index (Pearson's r = 0.13; P < 10-5) or (g) the distance between cell bodies (Pearson's r = -0.053; P = 0.0021).

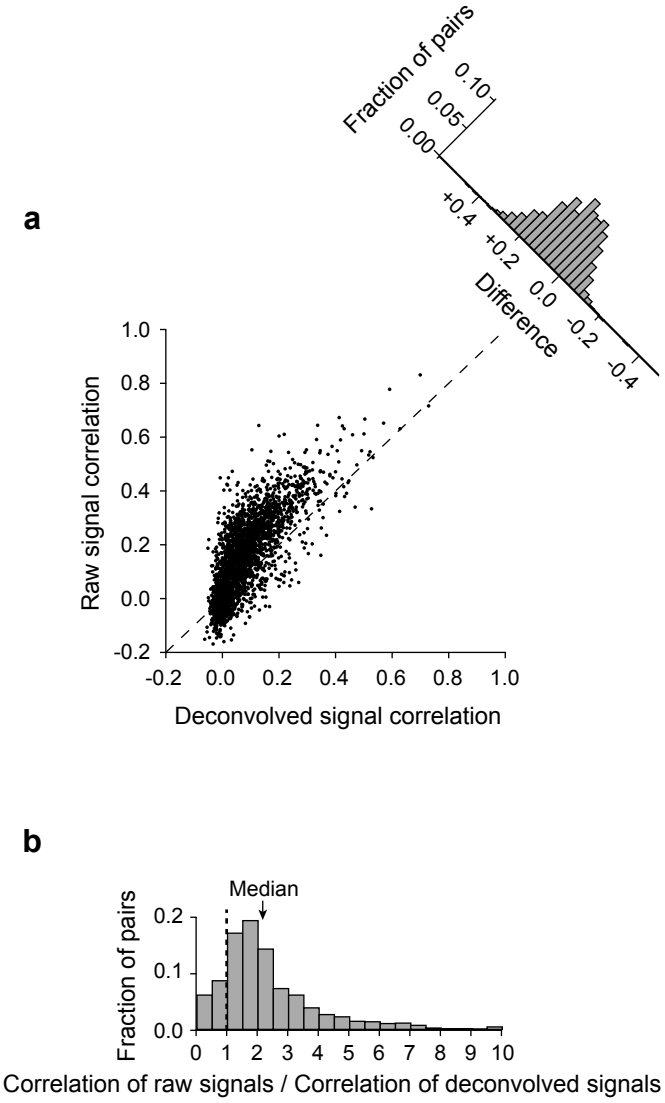

Supplementary Figure 6. Cross-correlations from raw fluorescence signals are higher than from deconvolved signals

(a) For the same set of neurons, we calculated the pairwise cross-correlations using raw fluorescence traces and deconvolution-based estimated spike rate time courses (n = 1101 pairs). (b) Cross-correlation values obtained from raw fluorescence signals were greater than those obtained from estimated spike rate time courses. In many cases the difference was over 2-fold.

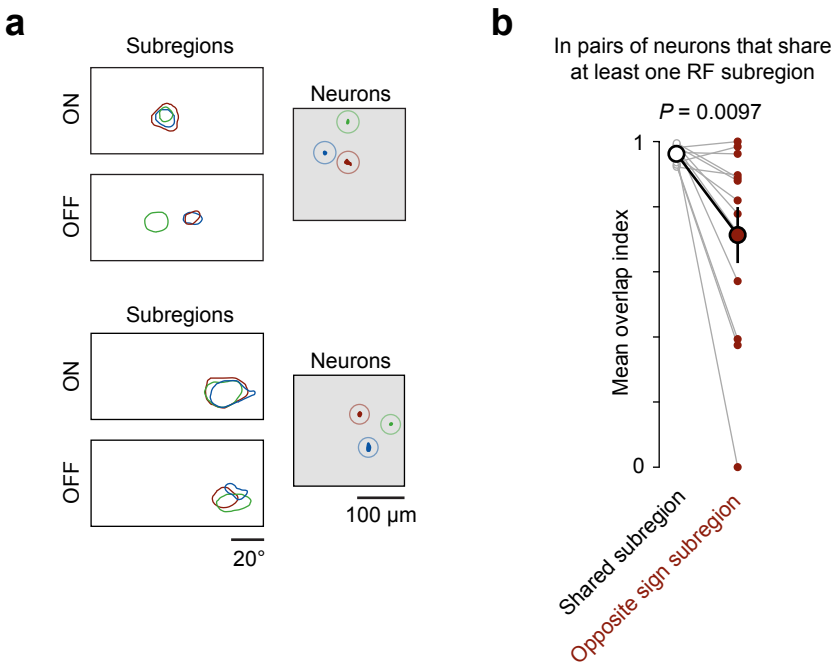

Supplementary Figure 7. Neurons that share one RF subregion, have subregions of the opposite sign that overlap less

(a) Example cells are shown, with both their ON and OFF RF subregions. Note that the lower group of cells is the same shown in bottom of Fig. 4a. Here, both the ON and OFF RF subregions are shown. (b) Subregions that are shared overlap to a high degree, but in those same cells, subregions of the opposite sign overlap less (*P*=0.0097, paired t-test, n=13). Note that high overlap is only one of the three criteria for shared RF subregions. The opposite sign subregions with high overlap indices differed in size and/or were centered on different points in visual space, and thus were not shared.

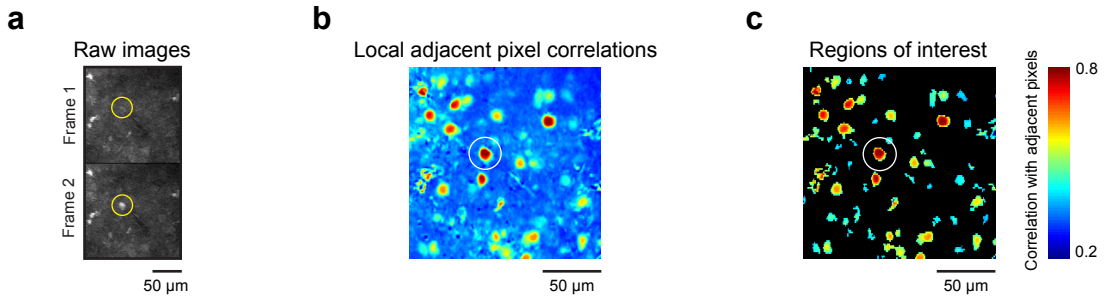

Supplementary Figure 8. Automated identification of regions of interest

(a) In the first of two adjacent frames (at 15.6 frames/s acquisition), the circled neuron appears with very low contrast against the background (Frame 1), but during a spike in the next frame the neuron was clearly visible (Frame 2). Therefore, instead of using an average signal to define regions of interests, we used the entire spatiotemporal data set. (b) The temporal cross-correlation of each pixel with its adjacent neighbors was used to identify putative neurons and processes. (c) The local cross-correlation image was then filtered with an adaptive local threshold. Finally, a series of morphological filters were used to define candidate neuron locations.

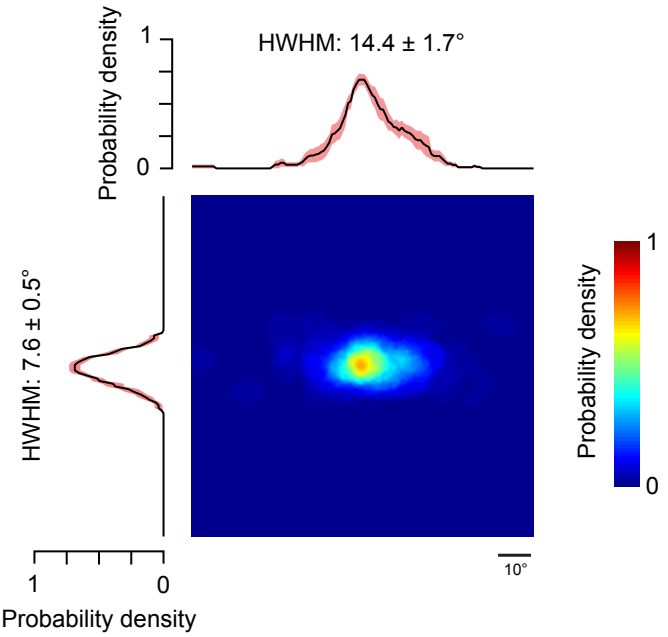

Supplementary Figure 9. The average subregion sampling of visual space

After obtaining the RFs for a local population of neurons in visual cortex (over the 230 x 230 µm imaging region), we plotted all subregions in one visual space. In order to combine data form multiple animals, the center of mass of each ensemble (ON or OFF) was centered at the origin (0,0). Next, the ensembles for all animals were averaged together. The resulting map is significantly elongated in the horizontal axis. This is likely related to the smaller cortical magnification factor observed for azimuth (~0.01 mm/°) compared to elevation (~0.02 mm/°) in mouse monocular cortex, observed in both intrinsic imaging (Kalatsky and Stryker, 2003) and extracellular recording (Wagor et al., 1980).

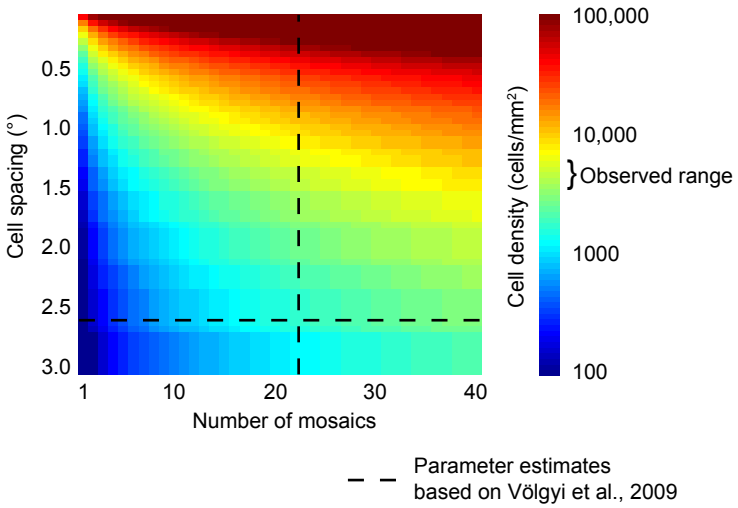

Supplementary Figure 10. Retinal ganglion cell density as a function of mosaic spacing and number of mosaics

Using an estimate of retinal magnification factor (31 µm/°; Remtulla and Hallett, 1985), and assuming retinal mosaics with a small amount of noise matched to observed data (Wassle et al., 1981), the density of retinal ganglion cells has been computed as a function of the number of mosaics and cell spacing within each matrix. The observed range of cell density (Drager and Olsen, 1981; Salinas-Navarro et al., 2009) is indicated on the logarithmic color scale bar. The dotted lines indicate the parameter estimates based on a recent survey of mouse retinal ganglion cell types (Völgyi et al., 2009). The number of different cell types was based on anatomical classification, the cell spacing was estimated here as 1.25 * average dendritic tree radius reported for the 22 cell types identified in the study. Note that the estimated parameters fail to account for the full cell density observed in retinal ganglion cell counting studies by a factor of 5 – 8.

Supplementary Note 1
Low firing rates can reduce correlation coefficients

The Fano Factor (variance-to-mean ratio) of sparse noise movie-evoked spike trains obtained during on-cell recordings was 1.34. This value indicates a slight tendency for "burstiness", but is close to 1. A prior study on mouse visual cortex concluded that the Fano factor for layer 2/3 neurons was variable, but on average indistinguishable from 1.0 (ref. 1). Thus we will use Poisson statistics as an approximation of the true spiking probability distributions.

Each stimulus frame was displayed for approximately 333 ms and the peak spike rate observed in our on-cell recordings for such an interval was 3.54 ± 2.18 spikes/s (mean ± SD, n = 19). Thus, for a highly preferred frame that evokes a peak spike rate, within a duration of 333 ms, a mean of 1.18 spikes is expected. The probability of observing no spikes (1 - $P_{response}$) is:

$$P_r(n) = \frac{r^n e^{-r}}{n!}$$ (Poisson distribution)

Where r is the mean count (1.18 spikes) and $P_r(n)$ is the probability of observing n spikes, given the mean rate r. This yields a probability of 0.31 for observing zero spikes in response to a preferred stimulus, or a response probability of just 0.69. Given two identical neurons, each receiving identical input, the probability of them both responding to the same stimulus presentation is 0.48. This shows how the low spike rates can limit the maximal correlation coefficients to values much less than 1.0. Note that this estimated upper limit for correlations matches the maximal values of correlations we have observed (Supplementary Fig. 5).

These low correlations, together with the low probability for sharing both ON and OFF RF subregions (Supplementary Fig. 7), indicates that groups of neurons that share a subregion do not represent redundant units of cortical circuitry.

Supplementary Note 2

An estimate of the number of RGCs afferent to the portion of visual cortex in the field of view

We have used the following equations, together with known parameters of the mouse visual system, to estimate an upper bound on the number of RGCs that encode the same area of visual space as the area of visual cortex we imaged, giving 1270 RGCs.

$$N_{RGC} = D_{RGC} * A_{retina} \quad \text{(Eq. 1)}$$

$$A_{retina} = (\frac{X_{im}}{m_{cortex,X}} * m_{retina}) * (\frac{Y_{im}}{m_{cortex,Y}} * m_{retina}) \quad \text{(Eq. 2)}$$

Symbol	Parameter	Value or equation
N_{RGC}	Number of RGCs	Eq. 1
D_{RGC}	Density of RGCs	5000 (refs. 2, 3)
A_{retina}	Area of retina that encodes the same area of visual space encoded by the portion of visual cortex imaged	Eq. 2
X_{im} Y_{im}	X (azimuth) and Y (elevation) dimensions of the visual cortex imaged	230 µm (for both X_{im} and Y_{im})
$m_{cortex,X}$ $m_{cortex,Y}$	Cortical magnification factor for azimuth (X) and elevation (Y)	0.01 mm/° (azimuth) and 0.02 mm/° (elevation) (refs. 4, 5, also see Supplementary Fig. 7)
m_{retina}	Retinal magnification factor	31 µm/° (ref. 6)

We call this an upper bound for several reasons:

(1) The estimated number of retinal mosaics (~20, ref. 7) and the spacing within these mosaics (estimated to be equal to the dendritic tree radius, which is at the dense end of reported mosaics[8, 9] result in cell densities approximately 5-10 fold less than what is observed in RGC cell counts (see Supplementary Fig. 10). Therefore, there may be many more mosaics to be discovered, or the spacings of those mosaics are even denser than estimated here. Alternatively, RGC counting methods may overestimate of the RGC population.

(2) Some RGC types will not project to V1-projecting relay neurons in the dorsal lateral geniculate nucleus.

(3) Some RGC types may not respond strongly to our visual stimulus and thus will not appreciably contribute to our measured receptive fields.

Supplementary Note 3

Retinal ganglion cell mosaics and their potential influence on V1 receptive fields

Retinal ganglion cells (RGCs) of a given type form a regular mosaic and tile the retina, resulting in homogeneous coverage. Since each RGC type forms its own mosaic, the nearest-neighbor distances among RGCs of different types are typically smaller than those among RGCs of the same type[9]. This characteristic spacing between RGCs has motivated a model of cortical development which shows that this feature can play a key role in influencing the structure of V1 receptive fields and orientation columns in cats[9-12].

Similar to how RGC mosaics could influence V1 receptive fields in cats, the shared V1 RF subregions we have observed may be a direct geometric consequence of RGC mosaics. Specifically, shared RF subregions could be due to shared input originating from a small number of RGCs, which is consistent with a prediction for rodents[11]. Specifically, a large amount of subregion overlap and a low degree of convergence have been suggested as a way in which the model might be extended to rodents[11].

In cats, the model predicts that neighboring V1 cells will sample from very similar populations of RGC RFs[10]. The large magnification factor allows for this, and the result is orientation columns. In rodents, neighboring V1 cells will sample from a more diverse set of RGC RFs due to the small magnification factor. The result is a salt-and-pepper orientation map[13]. However, the magnification factor is not so small as to avoid occasional resampling of the same afferents, and this manifests itself as shared RFs.

Similarly, the offset coverage of ON and OFF RF subregions within a local population could be due to the low degree of divergence in the mouse visual pathway and a relatively small population of RGCs contributing to V1 RF subregions. With small samples of ON and OFF RGC RFs, spatial inhomogeneities may be exaggerated. Thus, these two features of RFs in local populations of mouse V1 may be a direct consequence of RGC mosaics.

Supplementary Note 4
Comparison of divergence in the cat and mouse visual pathways

In addition to the potentially common aspects of visual processing in mice and other species, there are special aspects of the mouse visual pathway that may influence the features we observed. The layer 2/3 neurons we imaged were found to have non-overlapping ON and OFF RF subregions, indicating that they are simple cells, consistent with results from extracellular recording in mice[1, 14]. By contrast, in the cat, layer 2/3 neurons are typically complex[15] and exhibit overlapping ON and OFF RF subregions[16].

Another difference is that the large degree of divergence in the cat visual pathway is not present in mice. In the cat, dorsal lateral geniculate nucleus (dLGN) cell counts are about 3.4 – 6.2 times those for retinal ganglion cells (RGCs)[17-22], and this supports divergence on the order of 10 (ref. 23). In the mouse, the situation is reversed, with RGC counts being about 2.7 times those for the dLGN[24], and since the convergence is known to be about 1 – 3 (ref. 25), the divergence is limited to the order of 1, since the ratio of divergence to convergence is equal to the ratio of the numbers of postsynaptic cells to presynaptic cells. However, like the cat, this synapse may exhibit cell-type specificity, with dLGN neurons receiving input from a single or a select group of RGC types[8, 26, 27].

The thalamocortical connection is another source of divergence in the cat visual system, with about 450 mm^2 of cortical area[28, 29] receiving input from approximately 500,000 dLGN neurons[17, 18]. In the mouse, about 2 mm^2 of cortex[4, 30] receives input from approximately 10,000 dLGN neurons[24], so although the cat has 50-fold more dLGN neurons, it also has 225-fold more cortical area for primary visual cortex (V1) than the mouse. The low degree of divergence in the mouse visual system is an important difference between the cat and mouse visual systems and may contribute to the feature of shared RF subregions. Thus, shared RF subregions are more likely to be found in cortical areas with a low degree of divergence, such as intracortical projections, rather than the large divergence of cat V1.

References

1. Niell, C.M. & Stryker, M.P. Highly selective receptive fields in mouse visual cortex. *J Neurosci* **28**, 7520-7536 (2008).
2. Drager, U.C. & Olsen, J.F. Ganglion cell distribution in the retina of the mouse. *Invest Ophthalmol Vis Sci* **20**, 285-293 (1981).
3. Salinas-Navarro, M.*, et al.* Retinal ganglion cell population in adult albino and pigmented mice: a computerized analysis of the entire population and its spatial distribution. *Vision Res* **49**, 637-647 (2009).
4. Kalatsky, V.A. & Stryker, M.P. New paradigm for optical imaging: temporally encoded maps of intrinsic signal. *Neuron* **38**, 529-545 (2003).
5. Wagor, E., Mangini, N.J. & Pearlman, A.L. Retinotopic organization of striate and extrastriate visual cortex in the mouse. *J Comp Neurol* **193**, 187-202 (1980).
6. Remtulla, S. & Hallett, P.E. A schematic eye for the mouse, and comparisons with the rat. *Vision Res* **25**, 21-31 (1985).
7. Volgyi, B., Chheda, S. & Bloomfield, S.A. Tracer coupling patterns of the ganglion cell subtypes in the mouse retina. *J Comp Neurol* **512**, 664-687 (2009).
8. Huberman, A.D.*, et al.* Architecture and activity-mediated refinement of axonal projections from a mosaic of genetically identified retinal ganglion cells. *Neuron* **59**, 425-438 (2008).
9. Wassle, H., Boycott, B.B. & Illing, R.B. Morphology and mosaic of on- and off-beta cells in the cat retina and some functional considerations. *Proc R Soc Lond B Biol Sci* **212**, 177-195 (1981).
10. Ringach, D.L. Haphazard wiring of simple receptive fields and orientation columns in visual cortex. *J Neurophysiol* **92**, 468-476 (2004).
11. Ringach, D.L. On the origin of the functional architecture of the cortex. *PLoS One* **2**, e251 (2007).
12. Soodak, R.E. The retinal ganglion cell mosaic defines orientation columns in striate cortex. *Proc Natl Acad Sci U S A* **84**, 3936-3940 (1987).
13. Ohki, K., Chung, S., Ch'ng, Y.H., Kara, P. & Reid, R.C. Functional imaging with cellular resolution reveals precise micro-architecture in visual cortex. *Nature* **433**, 597-603 (2005).
14. Mangini, N.J. & Pearlman, A.L. Laminar distribution of receptive field properties in the primary visual cortex of the mouse. *J Comp Neurol* **193**, 203-222 (1980).
15. Gilbert, C.D. Laminar differences in receptive field properties of cells in cat primary visual cortex. *J Physiol* **268**, 391-421 (1977).
16. Martinez, L.M.*, et al.* Receptive field structure varies with layer in the primary visual cortex. *Nat Neurosci* **8**, 372-379 (2005).

17. Williams, R.W., Cavada, C. & Reinoso-Suarez, F. Rapid evolution of the visual system: a cellular assay of the retina and dorsal lateral geniculate nucleus of the Spanish wildcat and the domestic cat. *J Neurosci* **13**, 208-228 (1993).

18. Madarasz, M., Gerle, J., Hajdu, F., Somogyi, G. & Tombol, T. Quantitative histological studies on the lateral geniculate nucleus in the cat. II. Cell numbers and densities in the several layers. *J Hirnforsch* **19**, 159-164 (1978).

19. Stone, J. A quantitative analysis of the distribution of ganglion cells in the cat's retina. *J Comp Neurol* **124**, 337-352 (1965).

20. Stone, J. & Campion, J.E. Estimate of the number of myelinated axons in the cat's optic nerve. *J Comp Neurol* **180**, 799-806 (1978).

21. Illing, R.B. & Wassle, H. The retinal projection to the thalamus in the cat: a quantitative investigation and a comparison with the retinotectal pathway. *J Comp Neurol* **202**, 265-285 (1981).

22. Hughes, A. A quantitative analysis of the cat retinal ganglion cell topography. *J Comp Neurol* **163**, 107-128 (1975).

23. Yeh, C.I., Xing, D., Williams, P.E. & Shapley, R.M. Stimulus ensemble and cortical layer determine V1 spatial receptive fields. *Proc Natl Acad Sci U S A* **106**, 14652-14657 (2009).

24. Coleman, J.E., Law, K. & Bear, M.F. Anatomical origins of ocular dominance in mouse primary visual cortex. *Neuroscience* **161**, 561-571 (2009).

25. Chen, C. & Regehr, W.G. Developmental remodeling of the retinogeniculate synapse. *Neuron* **28**, 955-966 (2000).

26. Huberman, A.D.*, et al.* Genetic identification of an On-Off direction-selective retinal ganglion cell subtype reveals a layer-specific subcortical map of posterior motion. *Neuron* **62**, 327-334 (2009).

27. Kim, I.J., Zhang, Y., Meister, M. & Sanes, J.R. Laminar restriction of retinal ganglion cell dendrites and axons: subtype-specific developmental patterns revealed with transgenic markers. *J Neurosci* **30**, 1452-1462.

28. Rathjen, S.*, et al.* The growth of cat cerebral cortex in postnatal life: a magnetic resonance imaging study. *Eur J Neurosci* **18**, 1797-1806 (2003).

29. Rathjen, S., Schmidt, K.E. & Lowel, S. Postnatal growth and column spacing in cat primary visual cortex. *Exp Brain Res* **149**, 151-158 (2003).

30. Drager, U.C. Receptive fields of single cells and topography in mouse visual cortex. *J Comp Neurol* **160**, 269-290 (1975).